Data analysis of the TetraSpar demonstrator measurements

Singh, D.; Haugen, Erik; Laugesen, Kasper; Chauhan, Ayush; Viré, A.C.

DOI
10.1088/1742-6596/2767/6/062025

Publication date
2024

Published in
Journal of Physics: Conference Series

Data analysis of the TetraSpar demonstrator measurements

Journal of Physics: Conference Series **2767** (2024) 062025 doi:10.1088/1742-6596/2767/6/062025

Data analysis of the TetraSpar demonstrator measurements

Deepali Singh[1], Erik Haugen[2], Kasper Laugesen[3], Ayush Chauhan[4], Axelle Viré[1]
[1] Delft University of Technology, Kluyverweg 1, 2629 HS Delft, The Netherlands
[2] Siemens Gamesa Renewable Energy, Tonsbakken 16, 2740 Skovlunde, Denmark
[3] Siemens Gamesa Renewable Energy, Borupvej 16, 7330 Brande, Denmark
[4] Siemens Gamesa Renewable Energy, 560020 Bangalore, India

E-mail: d.singh-1@tudelft.nl

Abstract. Floating offshore wind turbines can extract energy from deep offshore locations, typically unfit for fixed bottom designs. The complex interaction between the structural behavior of the floating offshore wind turbine and the stochastic site conditions, however, is an active area of research. Characterizing the relationship between the environmental conditions and loads may help design reduced-order models, surrogate models, and physics-based engineering models for floating wind turbines. This study uses data from the TetraSpar prototype equipped with a 3.6 MW Siemens Gamesa wind turbine. One-to-one simulations performed using an aero-servo-hydro-elastic software are included for comparison. Various tools, including linear correlation, mutual information, feature ordering using conditional independence, and sensitivity analysis using a data-driven variogram fit, are used for the assessment. This study is also helpful in validating the engineering model for future global sensitivity analysis using elementary effects or Sobol indices that require a rigid sampling of features and can, therefore, only be calculated with simulation tools. We find a good agreement between the experiments and simulations. The 10-min. damage equivalent loads on the tower show a correlation, particularly with the wind speed statistics and the significant wave height.

1. Introduction

Floating offshore wind turbines offer a vast potential to extract energy from deep offshore regions with stronger and more consistent wind resources. However, the interaction between the floating system and the stochastic site conditions, which ultimately results in uncertainty in the structural response, still needs to be better understood. Sensitivity and correlation analyses are valuable for designing structures with smaller safety factors and for feature selection for developing engineering, reduced order, and data-driven surrogate models. Several studies in the past have focused on addressing the sensitivity of wind turbine loads to environmental conditions [1, 2, 3, 4, 5]. The combined effect of environmental and structural parameters has been analyzed on fixed-bottom [6, 7] and floating wind turbines with semi-submersible platforms [8, 9]. However, in the case of floating wind turbines, the response is also a function of the substructure type [10]. This means that the sensitivity analysis for semi-submersibles may not be completely relevant for the spar.

This study relies on the measurements obtained from the TetraSpar demonstrator [11, 12], equipped with a 3.6MW Siemens Gamesa Renewable Energy wind turbine. An image of the

platform with the wind turbine is shown in Figure 1. The TetraSpar prototype has been installed at the Marine Energy Test Centre, 10 km off Karmøy in Norway, at a depth of 200 m and has been operating since July 2021 [12]. The objective of this paper is to perform a Global Sensitivity Analysis (GSA) and a correlation study between 10-minute statistics of environmental conditions and the corresponding 10-min. damage equivalent loads (DELs), also referred to as short-term DELs (STDEL) or 10-min. DEL, obtained from the measurement campaign.

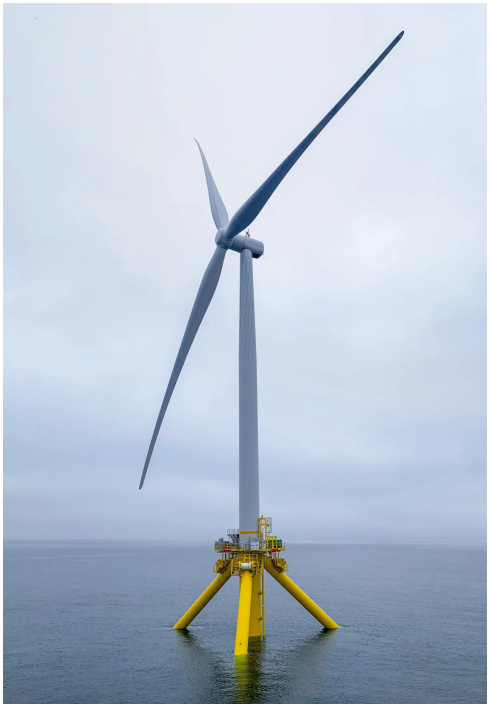

Figure 1: Image of the TetraSpar full-scale demonstrator moored at the test site off the coast of Norway. [12]

GSA on wind turbines is generally performed using either a derivative-based approach, such as elementary effects, or a variance-based approach, such as Sobol's indices. Both approaches suffer from a few significant issues [13]. First, they follow a rigid sampling strategy. Second, they require a function to evaluate the input-output relationship - in this case, a relatively expensive engineering tool such as OpenFAST. Therefore, they cannot be used on randomly sampled field measurement data. Additionally, the analysis implicitly reflects any deficiencies the numerical model may have. Performing GSA using either of the two approaches on field measurement data necessitates fitting a surrogate model to the observations, followed by sampling the responses to perform a GSA using traditional methods.

We perform GSA with the recently introduced data-driven variogram analysis of response surfaces (D-VARS) [13] to address these issues. For the correlation study, we evaluate the conditional dependence coefficient (CODEC) and a corresponding variable selection algorithm called Feature Ordering by Conditional Independence (FOCI)[14]. Other standard correlation metrics, including mutual information (MI) and Pearson's correlation coefficient (PC), are also evaluated.

An extension of this study would be to use traditional GSA techniques like elementary effects or Sobol's sensitivity indices that require a uniform and organized sampling of parameters. Simulation tools play an essential role in performing GSA studies, as this is not possible with site measurements. In order to validate the extent to which we can rely on the state-of-the-

art engineering tools used in the industry to perform such analyses, one-to-one simulations are carried out using the in-house multi-physics tool, BHawC [15, 16] coupled with OrcaFlex. The correlation studies are repeated on measured and simulated data; the comparison is presented in this paper.

The details of load acquisition from the measurement campaign and the pre-processing performed before running the analysis are presented in Section 2. The simulation setup is presented in Section 3. A brief note on the statistical methods is presented in Section 4 followed by results and discussion in Section 5.

2. Parameters and data pre-processing

2.1. Parameters

The Tetraspar prototype is heavily instrumented, with the sensors on board providing data to a central data acquisition system, which stores data at a frequency of 25 Hz. The turbulence intensity, wind speed at hub height, and shear profile are processed from the nacelle-based LiDAR measurements. The free-stream wind conditions are measured 364 m upstream of the rotor plane. The onboard wave radar measures the wave elevation and direction, which are then processed to obtain values of significant wave height and peak spectral frequency. The wave radar is located at the base of the tower, targeting the area directly below the wind turbine. It is, therefore, subject to additional disturbances due to the surrounding floating structure compared to the open ocean. Ocean current characteristics in the form of current speed and direction are not measured directly at the location and are obtained from the Norwegian Meteorological Institute's reanalysis data. Air density is derived from temperature measurements.

The quantities of interest (QoI) are the loads measured at the blade root, tower top, and tower bottom. The high-frequency sensor measurements are processed to obtain 10-minute load statistics. The input parameters considered for this study are listed in Table 1. The periods of normal operation are selected and processed to remove any faulty sensor measurements between 3 March 2022 and 31 October 2022.

Variable	**Source**
Turbulence intensity, hub height mean wind speed, shear profile power law exponent	Nacelle-based LiDAR
Air density	Derived from temperature
Platform pitch angle	Inclinometer (tower top)
Significant wave height, wave elevation peak frequency, wave direction	Wave Radar
Current speed, Current direction	Meteorologisk Institut (met.no)

Table 1: List of variables characterizing the environmental conditions

2.2. Data processing

The filtered 10-minute measurements and simulation output are further processed to render them suitable for our statistical analysis tools.

- **Missing values**: For any missing measurement channel in the dataset, all measurements from that timestamp are discarded.
- **Acquisition frequency**: Current speed, current direction, and density are recorded every hour, and therefore, their values repeat over a period of time until the next acquisition point. This does not introduce an issue with MI and PC. However, the repeated values can

introduce an artificial bias in the data for CODEC, FOCI, and D-VARS. Therefore, the CODEC, FOCI, and D-VARS analysis is performed on a much smaller dataset where the repeating values of density, current speed, and current direction are discarded.

- **Outlier detection**: CODEC, FOCI, and D-VARS analysis has an additional outlier detection step. We use a simple metric called the *z-score* to mark any sample more than 2.5 standard deviations away from the mean as an outlier. For the i^{th} data sample with value x_i, the z-score value is defined as

$$z_i = \frac{(x_i - X.mean)}{X.std} \tag{1}$$

  where X is a vector of the parameter values.
- **Normalization**: Both simulation and measurement channels are normalized between the min and max values of the measurements (X_{meas}) per channel,

$$x_{inorm} = \frac{x_i - X_{meas}.min}{X_{meas}.max - X_{meas}.min} \tag{2}$$

After filtering and processing the data, we are left with roughly 9489 10-min. samples to perform MI and PC. The number of samples was further reduced to 1145 for CODEC, FOCI, and D-VARS analysis. With the limited amount of noisy data to perform the analysis, we expect statistical uncertainty in the estimates.

2.3. STDEL calculation

Rainflow counting [17] algorithm is used to obtain the load ranges S_i and the number of load cycles n_i needed to calculate the $STDEL$ as,

$$STDEL \coloneqq \left(\frac{n_i S_i^m}{n_{ref}}\right)^{1/m}, \tag{3}$$

where n_{ref} is 600 for 1Hz DELs over 10 minutes. m is the Wöhler coefficient with values 3.5 for the tower, 10 for blade flapwise, and 8 for blade edgewise moments.

3. Simulation setup

BHawC, or Bonus Horizontal Axis Wind Turbine Simulation Code, is an in-house aero-servo-elastic solver developed by Siemens Gamesa Renewable Energy. It is dynamically coupled with the hydrodynamic solver, OrcaFlex, which models the platform hydrodynamic loads and mooring loads and response. At each coupling step, BHawC calculates the aero-servo-elastic response, providing OrcaFlex with the displacement, velocity, and acceleration of the interface between the tower and foundation. With these inputs, OrcaFlex calculates the hydro-elastic response of the floater-mooring system at the interface location. The total simulation duration per simulation is set to 600 s, to match the 10-min. statistics from the prototype measurements.

The Mann model [18] is used to generate spatially coherent turbulent flow structures in the inflow. It uses a frozen-Taylor assumption to represent a wind time series as a spatial wind field. The turbulence box is scaled based on the wind speed, turbulence intensity, and the shear profile values which are obtained from the measurement campaign. The statistical variation in the turbulent field is reproduced by using different random seeds (ranging from 1 to 45) for the simulations.

The double-peaked Torsethaugen wave spectrum [19] is chosen to generate stochastic waves in OrcaFlex. It represents sea states that include both swell and wind-generated waves. An interpolated current profile is specified, based on the reanalysis data from the Norwegian

Meteorological Institute. The suspended keel and tubular structures are modeled as stacked spar-buoy cylindrical elements under the category of 6-D buoys in OrcaFlex. The mooring line dynamics are solved using a finite element model by discretizing the line into a series of lumped mass nodes connected by straight massless segments with axial and torsional spring dampers at each end.

4. Methodology

The measured data is of the form $\mathcal{D} = (\boldsymbol{x}_i, y_i), i = 1...n$ where $\boldsymbol{x_i} \in \mathbb{R}^m$ is the m-dimensional input vector of the sample i and $y_i \in \mathbb{R}$ is the corresponding response. It can be assumed that the data samples are realizations of random variables, input $\boldsymbol{X} = (X_j)_{1 \leq j \leq m}$ and response Y.

4.1. Pearson's correlation coefficient

Pearson's correlation (PC) is a simple measure of linear correlation between two random variables X and Y. The values of PC is bound by -1 and 1. 0 denotes a lack of linear correlation, whereas the negative and positive values are interpreted as inverse and direct linear relationship between the variables, respectively. Mathematically, it is expressed as,

$$r = \frac{\sum_{i=1}^{n}(x_i - \bar{x})(y_i - \bar{y})}{\sqrt{\sum_{i=1}^{n}(x_i - \bar{x})^2}\sqrt{\sum_{i=1}^{n}(y_i - \bar{y})^2}} \tag{4}$$

4.2. Mutual Information

MI is defined as a measure of the amount of information shared between two random variables. In other words, it measures the reduction in uncertainty of a random variable Y, given the knowledge of another random variable X. The value of mutual information ranges from 0 (complete independence) to a positive maximum (perfect correlation). The value itself is a function of the units of measurement of the quantities in question. In practice, it is symmetric, capable of measuring non-linear correlations and is not sensitive to outliers, making it a robust metric. For discrete variables X and Y with a joint probability distribution $P_{XY}(x, y)$, and marginal distributions $P_X(x), P_Y(y)$, it is defined as [20],

$$I(X;Y) = \sum_{y \in Y}\sum_{x \in X} \log\left(\frac{P_{X,Y}(x,y)}{P_X(x)P_Y(y)}\right) \tag{5}$$

4.3. Conditional dependence coefficient and feature ordering by conditional independence

CODEC is defined as the measure of conditional dependence of Y on a set of random variables $\boldsymbol{A}_{\{1...q\}}$ given a set of other random variables $\boldsymbol{B}_{\{1...p\}}$ [14], where p and $q \geq 0$. It is a fully non-parametric approach that can be used with randomly sampled, unstructured data, allowing us to use it on measurements directly. Two major advantages of CODEC include a fixed range from 0 to 1, and accounting for the conditional dependence between the various features. The coefficient is defined in Equation (6).

$$T(Y, \boldsymbol{A} \mid \boldsymbol{B}) = \frac{\int \mathbb{E}\left(\mathrm{Var}\left(\mathbb{P}(Y \geq t \mid \boldsymbol{A}, \boldsymbol{B}) \mid \boldsymbol{B}\right)\right)\mathrm{d}\mu(t)}{\int \mathbb{E}\left(\mathrm{Var}\left(1_{\{Y \geq t\}} \mid \boldsymbol{B}\right)\right)\mathrm{d}\mu(t)} \tag{6}$$

The value of T is estimated in the form of T_n for n discrete samples [14] as the exact value is not tractable. μ is the law of the random variable Y and $1\{Y \geq t\}$ is the indicator of the event Y greater than or equal to a threshold t.

On our data, FOCI uses CODEC for feature ordering as follows. First, the feature that maximizes $T_n(Y \mid X_j)$ is chosen from $j = j_1...j_m$, say, X_{j_1}. Then, the feature maximizing

$T_n(Y, X_j \mid X_{j_1})$ is chosen from the remaining features, $j \notin j_1$, say X_{j_2}. The feature maximizing $T_n(Y, X_j \mid X_{j_1}, X_{j_2})$ is chosen from the remaining features, $j \notin j_1, j_2$. This process is repeated k times until the value of $T_n \leq 0$. The subset of important features, thus, reduces to $\hat{S} = j_1 ... j_k$.

4.4. Data-driven variogram analysis of response surfaces

Variogram Analysis of Response Surfaces, VARS, is based on the idea that the variance in the response surface between any two points, $\boldsymbol{x}_1$ and $\boldsymbol{x}_2$, is a function of the distance $\boldsymbol{h}$ between the points in the m-dimensional input space. For $N(\boldsymbol{h})$ sample pairs, the semi-variogram γ can be approximated as:

$$\gamma(\boldsymbol{h}) = \frac{1}{2N(\boldsymbol{h})} \sum_{l=1}^{N(\boldsymbol{h})} (y(\boldsymbol{x}_l) - y(\boldsymbol{x}_l + \boldsymbol{h}))^2 \tag{7}$$

Sheikholeslami et al. [13] derive a form of the variogram based on the variance σ^2 and spatial covariance $C(\boldsymbol{h})$ of the response function, $\gamma(\boldsymbol{h}) = \sigma^2 - C(\boldsymbol{h})$.

For unstructured samples, Sheikholeslami et al. [13] introduce data-driven VARS, or D-VARS, that uses zero-mean Gaussian processes to obtain the covariances. In this study, we use a linear covariance function.

5. Results

The result section is divided into three parts. First, we compare the simulation predictions with measurements obtained from the prototype using scatter plots, MI, and PC. The scatter plots provide a qualitative comparison of the simulated and measured QoIs as a function of each of the environmental features. MI and PC provide a quantitative assessment of the degree of correlation between the fatigue loads as a function of the environmental conditions. Note that the variations in the response are a cumulative effect of changes in all the parameters. However, the correlation metrics disregard any conditional dependence between the input variables.

In the second part, we look at the results obtained using FOCI, which takes into account the conditional dependence between the input variables while calculating the score. The conditional dependence coefficient is helpful in determining a subset of interesting features that most explain the behavior of the QoI.

Finally, we assess the predictions obtained for the GSA using D-VARS. The ratios reflect the degree of variation in the response for a unit variation in the inputs.

5.1. Data visualization and standard correlation metrics

Figure 2 and Figure 3 show the 10-min. DEL plotted against the 10-minute statistics of the inflow quantities. Firstly, the simulations and measurements have a good qualitative agreement, and the statistical trends are similar. Regarding absolute values, the blade root edgewise DELs and tower DELs in simulations show a larger variance than the measurements. Subsequent investigation revealed a limitation in the structural modeling of the suspension lines connecting the upper floater section to the keel. In simulations, these suspension lines do not remain as taut as the prototype, primarily due to smaller structural damping. In certain cases, it results in artificially increased fatigue, especially in the non-damped side-side tower moment and the edgewise blade loads.

Figure 5 and Figure 6 show the MI and PC scores in measurements and BHawC simulations. For both tower bottom and top fatigue loads, the significant wave height and the mean and standard deviation of wind speed reflect a strong correlation. Meanwhile, the blade loads are mainly correlated to the wind statistics, especially the flapwise fatigue, which is turbulence-driven. We looked further into how flapwise fatigue correlates with significant wave height. Figure 4a shows the standard deviation of the measured platform pitch angle (measured at the

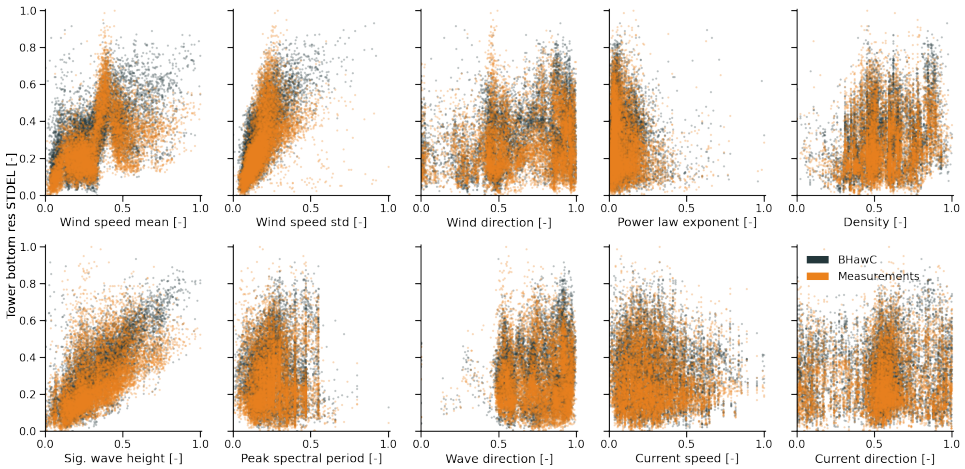

(a) Tower bottom resultant 10-min. DEL

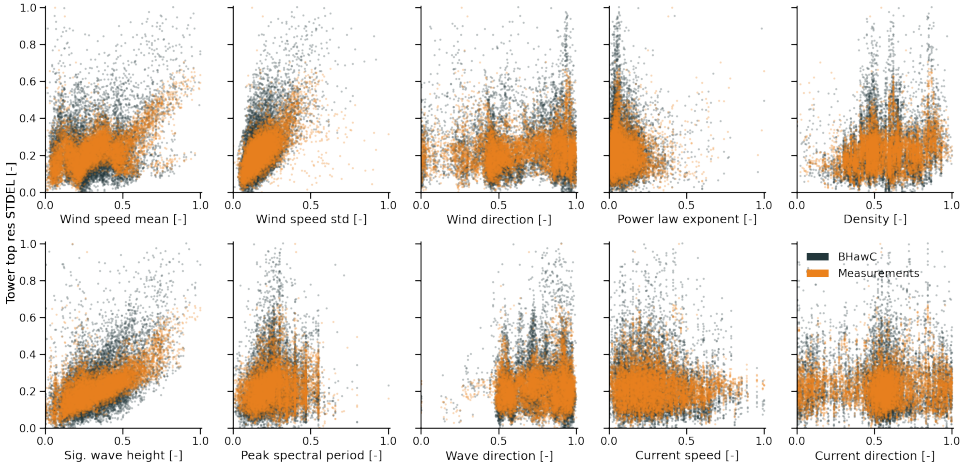

(b) Tower top resultant 10-min. DEL

Figure 2: Scatter plot of the 10-min. DELs calculated on the tower as a function of the environmental conditions.

tower top) plotted against the significant wave height. The color of each point corresponds to the mean wind speed, and its size reflects the wind speed standard deviation. Then, in Figure 4b, we show the blade root flapwise 10-min. DEL against platform pitch standard deviation. Here, point color represents significant wave height, and size reflects the wind speed standard deviation. We see in Figure 4b that higher blade root flapwise fatigue tends to occur when the significant wave height is high, and the standard deviation of hub height wind speed is large. The connection between significant wave height and flapwise fatigue might be influenced by the relationship between the platform pitch standard deviation and significant wave height, and how platform pitch standard deviation relates to flapwise fatigue. This is to show that it is difficult to account for the conditional dependence between all variables and trace a unique cause of fatigue damage. We also note that the tower top loads have a much stronger correlation in the measurement data with the significant wave height compared to BHawC.

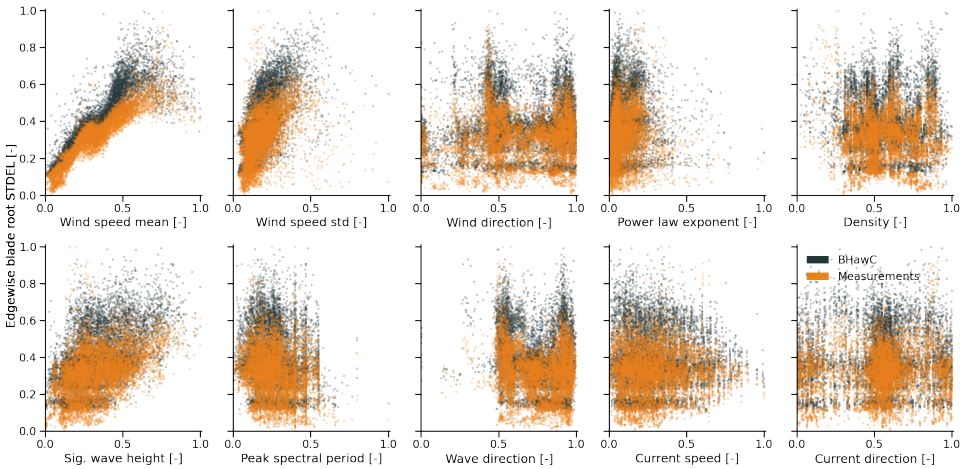

(a) Blade edgewise 10-min. DEL

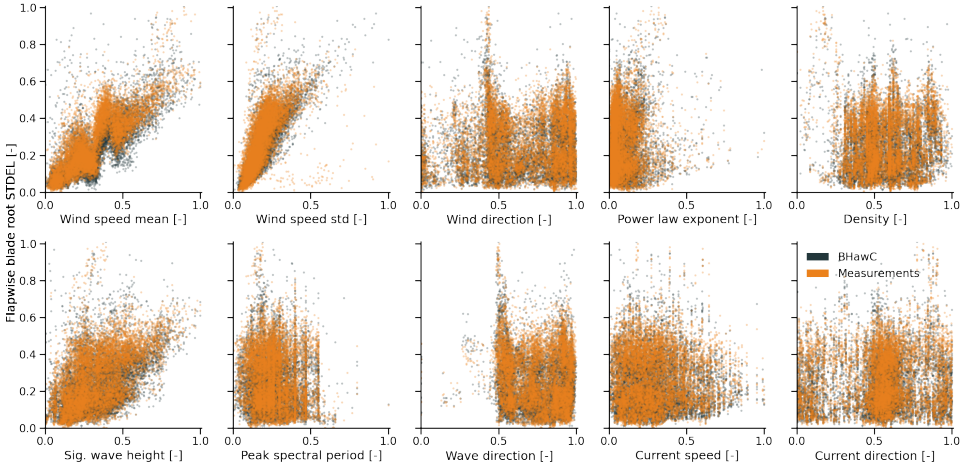

(b) Blade flapwise 10-min. DEL

Figure 3: Scatter plot of the 10-min. DELs calculated on the blade root as a function of the environmental conditions.

5.2. Feature ordering by conditional independence

Feature ordering is an essential pre-processing step in developing data-driven models. Table 2 shows the features chosen by this algorithm to contain the most information about the QoI. The values of the conditional dependence coefficient calculated with all the features versus those calculated with just the important features are also shown in the table. Note that the values of the coefficient range from 0 to 1; therefore, the closer the values to 1, the higher the chances of being able to predict the QoI using the information from the values of the important parameters. The most relevant features align with the trends seen in Section 5.1. Additionally, based on the values of the conditional dependence coefficient, C, we see that including non-important features in the dataset can lead to a reduction of the quality of information contained in it. Comparing the $C(Y|X(FOCI))$ values for this sample set, we would expect to have more success in training a data-driven model for predicting the blade root edgewise fatigue than the tower top resultant fatigue, as the latter is largely unexplained by the 10 environmental variables we have considered in this study. It must also be mentioned that FOCI uses the k-nearest neighbor algorithm for ranking the distances between the samples in practice. If two features are very close in relevance,

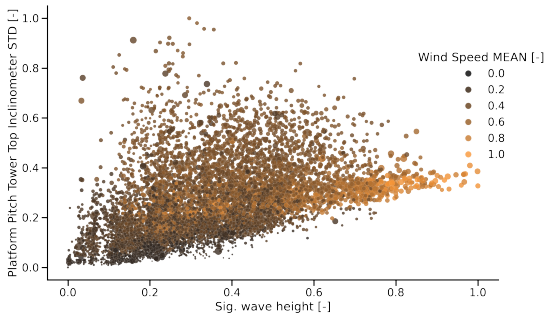

(a) The standard deviation of the platform pitch angle vs. the sig. wave height, shaded by the mean wind speed

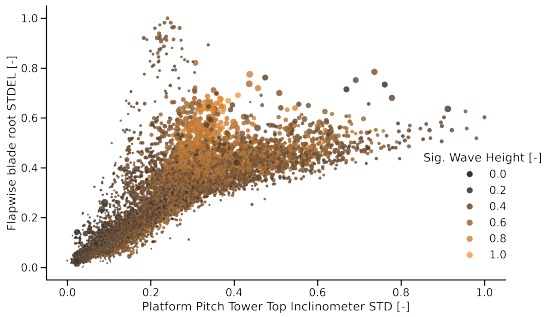

(b) Blade root flapwise 10-min. DEL vs. the standard deviation of the platform pitch angle, shaded by the sig. wave height

Figure 4: Scatter plots from the TetraSpar measurements, showing the influence of significant wave height on pitch and blade root flapwise moment 10-min. DEL. In all cases, the size of the symbols is based on the standard deviation of the wind speed.

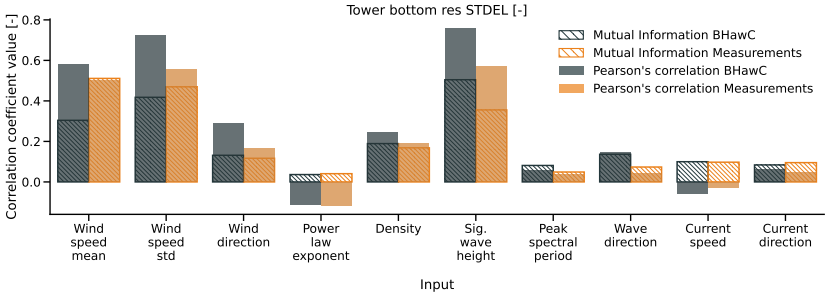

(a) Tower bottom resultant 10-min. DEL

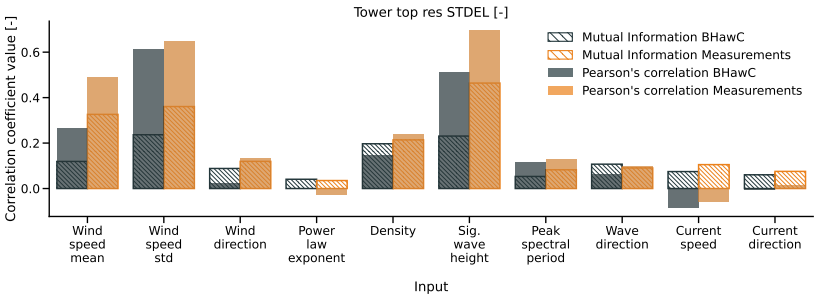

(b) Tower top resultant 10-min. DEL

Figure 5: MI and PC on tower loads for measurements and BHawC simulations

they may interchange their order of importance with changes in the dataset.

5.3. Variogram analysis

D-VARS fits an anisotropic variogram structure to the underlying response surface for a given dataset. The ratios shown in Figure 7 reflect the degree of sensitivity of the response to any change in the inputs, as we are utilizing the gradients of the response surface. The highest ratios for factor sensitivity follow a similar trend to the previous analyses, with the tower fatigue being

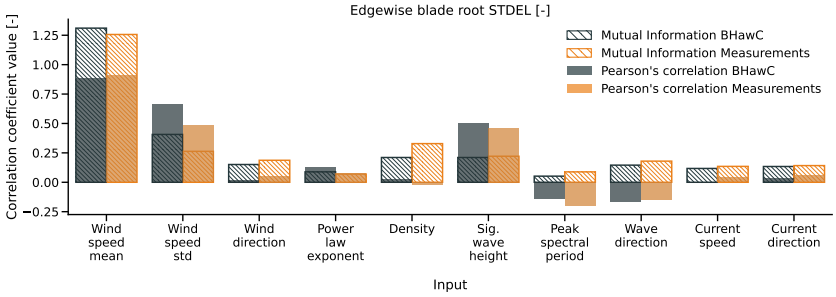

(a) Blade edgewise 10-min. DEL

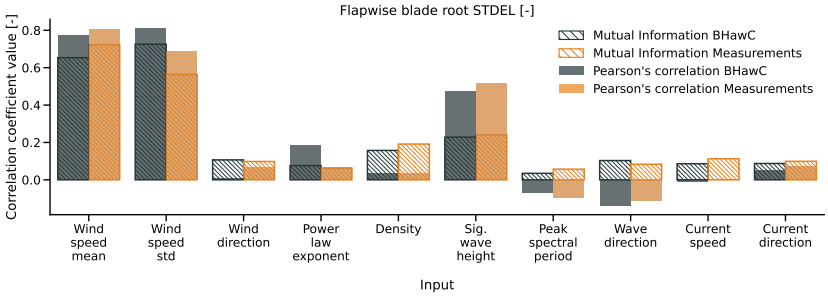

(b) Blade flapwise 10-min. DEL

Figure 6: MI and PC on blade root loads for measurements and BHawC simulations

Feature importance	Tower bottom res. STDEL	Tower top res. STDEL	Blade root edgewise STDEL	Blade root flapwise STDEL
1	Wind speed	Sig. wave ht.	Wind speed	Wind speed
2	Sig. wave ht.	Wind speed	Density	Wind speed std.
3	Wind speed std.	Wind speed std.	Sig. wave ht.	Density
4	-	Wave direction	-	-
$C(Y\|X)$	0.63	0.5	0.69	0.61
$C(Y\|X(FOCI))$	0.7	0.57	0.81	0.7

Table 2: Feature ordering using FOCI on the tetraspar measurement dataset

sensitive to the significant wave height and wind speed statistics. The current speed and direction are not shown to impact the tower and blade fatigue for this dataset significantly.

We found the method susceptible to statistical uncertainty based on the number of samples. It also did not seem robust to data outliers, and we noted that the presence of noise resulted in very flat response surfaces. Increasing the sample set in the future might reduce the uncertainty.

6. Conclusion

This study focused on the correlation and sensitivity analysis of the TetraSpar floating prototype equipped with a 3.6 MW Siemens Gamesa wind turbine. The goal was to understand the relationship between environmental conditions and the fatigue loads on the tower and blades, to aid in the development of data-driven reduced-order models and physics-based engineering models. Additionally, one-to-one simulations were performed using an aero-servo-hydro-elastic software (BHawC) for comparison with measured data.

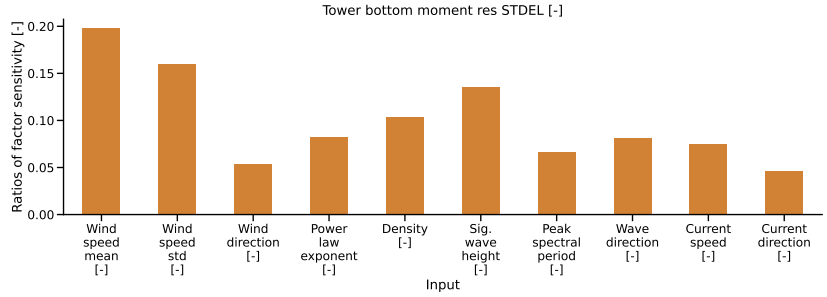

(a) Tower bottom resultant 10-min. DEL

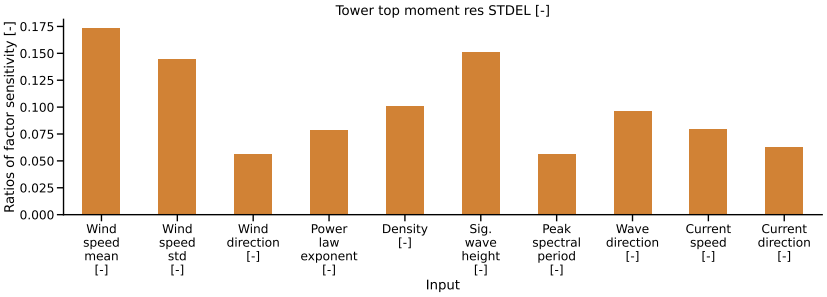

(b) Tower top resultant 10-min. DEL

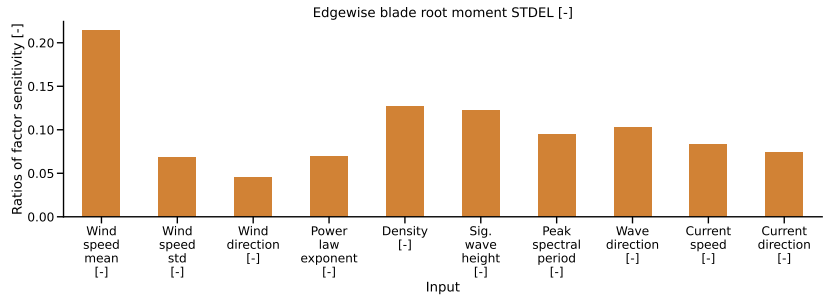

(c) Blade root edgewise 10-min. DEL

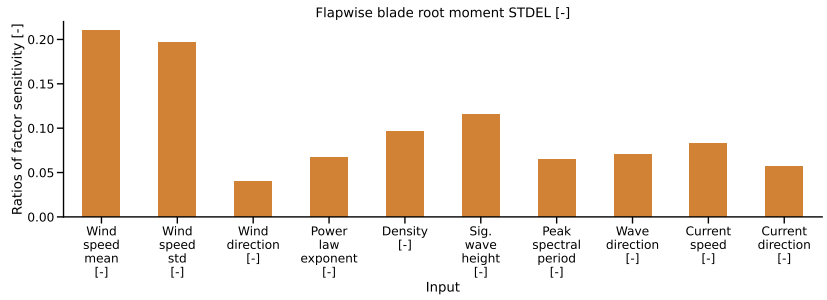

(d) Blade root flapwise 10-min. DEL

Figure 7: D-VARS performed on the 10-min. DEL at the tower and blade root

The scatter plots, mutual information, and Pearson's correlation coefficient revealed a good qualitative and quantitative agreement between the simulations and measurements. Significant wave height and wind speed mean and standard deviation were identified as the most important variables correlated to tower fatigue. Significant wave height was also found to give a correlation

with the blade root flapwise 10-min. DEL. Whereas, the edgewise fatigue loads were mainly driven by the mean wind speed, which in turn links to the rotor rpm and, therefore, to the cyclic gravitational loading. The mean current speed, profile and direction did not reveal any significant influence on the wind turbine fatigue. Further analysis could involve investigations on the mooring line tension drivers, which are expected to be current driven. Wind-wave misalignment would also be included as an additional parameter.

The FOCI algorithm provided valuable insights into feature importance, aiding in the identification of key parameters that significantly influence the response. The D-VARS analysis, despite showing promising results, highlighted some challenges related to statistical uncertainty and sensitivity to noise.

7. Acknowledgments

The project has received funding from the European Union's Horizon 2020 research and innovation program under grant agreement No. 860737 (STEP4WIND project, step4wind.eu).

References

[1] Robertson A, Sethuraman L, Jonkman J, Quick J 2018 *AIAA Wind Energy Symposium* AIAA 2018-1728
[2] Robertson A, Shaler K, Sethuraman L, Jonkman J 2019 *Wind Energ. Sci.* **4** 479-513
[3] Teixeira R, O'Connor A, Nogal M 2019 *Struct. Saf.* **81** 101860
[4] Shaler K and Robertson A and Jonkman J 2023 *Wind Energ. Sci.* **8** 25-40
[5] Sørum S H, Katsikogiannis G, Bachynski-Polić E, Amdahl J, Page A M, Klinkvort R T 2022 *Wind Energ.* **25** 1684-1709
[6] Hübler C, Gebhardt C G, Rolfes R 2017 *Renew. Energy* **111** 878-891
[7] Velarde J, Kramhøft C, Sørensen J D 2019 *Renew. Energy* **140** 177-189
[8] Wang Y, Lu Q, Yao T, Yin T, Zhao Y, Han Z, Xu Y, Jiang Z 2023 *Ocean Eng.* **285** 1-14
[9] Wiley W, Jonkman J, Robertson A, Shaler K 2023 *Wind Energ. Sci.*
[10] Edwards E C, Holcombe A, Brown S, Ransley E, Hann M, Greaves D 2023 *Renew. sustain. energy rev.* **183** 113416
[11] Borg M, Jensen M W, Urquhart S, Andersen M T, Thomsen J B, Stiesdal H 2020 *Energies* **13** 4911
[12] Stiesdal 2023 https://www.stiesdal.com/offshore/the-tetraspar-full-scale-demonstration-project/ (Accessed: 07 September 2023).
[13] Sheikholeslami R, Razavi S 2020 *Geophys. Res. Lett.* **47** e2020GL089829
[14] Azadkia M, Chatterjee S 2021 *Ann. Stat.* **49** 3070-3102
[15] Guntur S, Jonkman J, Sievers R, Sprague M A, Schreck S, Wang Q 2017 *Wind Energ. Sci.***2** 443-468
[16] Bussemakers M 2020 *Validation of aero-hydro-servo-elastic load and motion simulations in BHawC/OrcaFlex for the Hywind Scotland floating offshore wind farm* Delft: TU Delft http://resolver.tudelft.nl/uuid:5607a38d-6666-4cb3-9ebf-ba2a66a899fe
[17] Matsuishi M, Endo T 1968 *Jpn. Soc. Mech. Eng.* **68** 37-40
[18] Mann J 1998 *Probabilistic Eng. Mech.* **13** 269-282
[19] Torsethaugen K, Haver S 2004 *Int. Offshore and Polar Eng. Conf.* 2004-JSC-193
[20] Shannon C E, Weaver W 1949 *The Mathematical Theory of Communication* (Champaign: University of Illinois Press)